Preflight performance testing of the Multi-angle imaging SpectroRadiometer cameras

Carol J. Bruegge, Nadine L. Chrien, Barbara J. Gaitley, and Robert P. Korechoff
Jet Propulsion Laboratory, California Institute of Technology
4800 Oak Grove Dr., Pasadena, Ca. 91109

ABSTRACT

The Multi-angle Imaging SpectroRadiometer (MISR) will provide global data sets from Earth orbit using nine pushbroom cameras, each viewing in a fixed, unique direction. Data will be acquired for day-lit portions of the orbit at an average rate of 3.3 Mbits s^{-1} for the entire six year mission. Automated ground processing will make usc of the instrument radiometric, spectral, and geometric calibrations, 10 produce registered images at the nine view angles. This, the 1 .evel I product, provides top-of-atmosphere scene radiances, weighted by the spectral band profile for the instrument. Initially, processing will proceed with preflight determined radiometric response coefficients. In-flight radiometric calibration of the sensor will then provide monthly updates to these coefficients, to account for degradation which may occur during the mission. The spectral response profiles are invariant in time, and are provided only hy the preflight measurements. These include an out-of-band spectral calibration of each channel. These spectral data are used as input to the radiometric calibration of the instrument, and also to produce certain 1 .evel 2 products for which an out-of-band correction is made. This paper descri bes the calibration program, with emphasis on results from the recently completed preflight calibration.

1. INTRODUCTION

The MISR instrument has been designed and built by the Jet 1'repulsion Laboratory (JPL), (o be launched in 1998 as one of five instruments on the fi s(Earth Observing System platform (EO S-AM). It will fly in a 705 km (440 mile) sun-synchronous descending polar orbit, with an equatorial crossing time of 10:30 a.m. The instrument will be used to produce registered global data sets from nine camer as, spanning a range of view angles fi om nadi r to 70.5'" forward and aftward of nadir. The time separation from observation of a single ground target from the forward most camera to the aftmost view is 7 minutes. Within this lime the spacecraft covers a ground track 2800 km in length, with a swath width of 378 km. Each of the nine cameras images in four spectra] bands, specified at 443, 555, 670, and 865 nm (termed respectively Bands 1 -4). A charge-coLIplcd device (CCD) line array, 1504 active elements per line, underlies each of the four inter-fcrcacc filter strips. At the Earth's surface each detector element produces a data pixel with a cross-track spatial sampling interval of 275 m (250 m for the nadir camera). Additional samples of the video signal chain, termed overclock pixels, measure the video offset for each line of data.

2. TESTI NG OVERVIEW

The majority of preflight performance verification and calibration activities occur at the camera subsystem level[1-3]. (The camera subsystem provides signal detection and analog to digital conversion; the system electronics provide pixel averaging and square-root encoding). A pinhole target/ collimator assembly is used to determine modulation transfer function (MTF), poiat-spread function (PSF), camera boresight location, and pixel pointing (distortion)[4,5]. Radiometric testing makes usc of a 1 .65 m (65") integrating sphere, calibrated with high quantum efficiency light-trapped photodiodes. Twelve radiometric levels, unique to each spectral band and spanning the detector dynamic range, are used, Spectral calibration is conducted using a single-pms grating monochromator, xenon arc lamp, and variable width exit slit. Both in-band scans, at ().5 nm sampling and 2.6 am resolution, and out-of-band scans, at 19.6 nm resolution and 10 am sampling, are made of each CCD line array. Testing covers the 400" to 900 am range, but the response characterization is extended from 365 to 1 1()() nm through c(JIIIJloilcII1-level studies, '1'able 1 summarizes the performance testing results for the MISR cameras.

Satellite Remote Sensing ///, Proc. SPIE **2957**, Taormina, Italy, 23-26 September 1996

Table 1. Performance testing summary

Parameter	Specification	Performance
Modulation Transfer Function (MTF)	[).24 at 23.8 cycles per mm, beginning of life	1'21ss.
1 Effective focal length (EFL)	*59.3* (A), *73.4* (B), 95.3 (C), 123.8 (D) mm.	Verified to be within manufacture tolerance.
Camera boresight	Focal-plane center	Majority of cameras pass. Exceptions determined not to impact science products, as all boresights are sufficient to meet channel swath-overlap requirements. Scc Table *2* detail.
Distortion mapping	1/8 pixel pointing knowledge	Data delivered to specified accuracy.
Contrast target	Radiometric error less than 2% for *two* scene *types: 1)* an ocean half-plane adjacent to a cloudbank, and *2) a lake* within land surrounds.	Scene I pass; scene *2* found to have a I 0% error. Can meet requirement with image restoration algorithm. Makes usc of point-spread function (PSF) data, measured for each channel.
Saturation blooming	Radiometric effects negligible eight pixels distance from saturated pixel.	Image restoration algor ithm ineffective in neighborhood of saturated pixel, as peak signal is ofl-scale.
Signal-to-noise ratio (SNR)	100 at ρ_{eq}= *0.02*	Pass with large margin. 1)etectors are photon noise limited for much of range.
Absolute radiometric accuracy	3% (1σ) at ρ_{eq}= I 6% (1σ) at ρ_{eq}= 0.05	Gain coefficients deter-miacd. Error analysis demonstrates accuracy requirement met.
1 ,ocal uniformit y	3% standard deviation among consecutive four pixels	Majority pass with <1% deviation. Nine pixel sets have >10% response deviation, thus there is minimal science impact. Scc Table *2.*
Polarization insensitivity	± 1%	Pass. 1 ,yot depolarizer/ gaussian filter combination effective.
Spectral calibration	0.5 nm knowledge	Data delivered to specified accuracy.
Spectral center wavelength.	443, 555, 670, 865 ± 2 nm as determined from a total-band moments analysis.	Few channels meet the manufacture tolerance, duc to out-of-band response. Out-band correction provided for certain Level *2 products. Scc* Table *2.*
Spectral out-of-band	Specified at 1 $()^{-4}$ average and 10-3 peak response, Such that the integrated out/ in-band ratio is less than 1 %.	Found to be between 5 x 10^{-4} and 8 x 10^{-4}. Out-of-band correction provided for certain science products. Scc Table 2 detail.

Two parameters listed above are specified in terms of equivalent reflectance, ρ_{eq} (the measured radiance times π, divided by the band-weighted exo-atmospheric solar irradiance). This allows the specifications to be written using band-independent values.

In general the cameras were found to meet their design specifications. Exceptions, such as slight boresight and local non-uniformity errors, are believed to be small enough such that there is no effect on the science data products. Saturation blooming

affects are larger around the saturated pixel than originally anticipated. The cause may partially be explained by PSI', which appears broader because of the intense signal stren gth. This halo which cannot be effectively removed by PSF deconvolution, as the amount of energy to remove from neighboring pixels is unknown (the radiance falling on the saturated pixel is unknown). An electronic noise is additionally noted on pixels clocked out following the saturated element. This noise is negligible (-5 1)N out of the 16,384 DN range) for a single saturated pixel, but begins to be discernible when a large fraction of the array is saturated (the noise is additive with number of saturated pixels). This extended saturation scenario, however, is unlikely to occur on orbit.

A sophisticated data quality assessment algorithm will identify al] pixels which are radiometrically affected by saturation, or other specification errors. Pixels for which the specifications fail will not be used in science data product generation. Other data quality checks are for detector failures (e. g., poor signal-to-noise), or for pixels which have a low DN when the data line has an atypically high average DN. The latter is tracked, as at high ill umin ation levels it is noted that there is an uncertainty in the measured video offset. That is determined in that the overclock samples are not stable th roughout the line read. This electronic noise is also small (-25 DN for an average DN of 12,000 for the line), and therefore will seldom be problematic.

As Table I indicates, there are two performance violations that are more consequential and have resulted in added ground processing. That is, as a result of camera performance testing, MISR now plans to make use Of an out-of-band correction algorithm to certain 1 .evel 2 science products [7]. Additionally, an image restoration algorithm will use the measured PSF response to remove the effects of light scattering within the focal plane. These effects result from scattering within the filler, and between the detector and filter (separated by 38 μm)[8]. It should be kept in mind (bat MISR is calibrated to an unprecedented radiometric calibration accuracy (3%/1σ confidence level for uniform bright scenes). These added processing steps will allow spectrally 01' spatially inhomogeneous scenes to be measured within the radiometr ic specifications defined for more hom ogeneous scenes. Conversely, without (his processing the radiometric requirement would still be met for most scenes, however certain scene types would have radiance errors between 3 and 1()%.

'1'able 2 provides a breakdown of selected performance parameters, where camera-by-camera differences are of interest. Here lilt cameras arc identified using two naming con ventions. MISR data users will use the formalism that specifies a Camera by its lens type (A-D) and a "f" (forward), "n" (nadir) or "a" (aft) suffix depending on tile camel a location. As camera testing occurred prior 10 the assignment of camera locations on the instrument, a serial number tracked cacb cameras during the test phase. This convention uses the lens type, followed by three numbers representing the tens, focal plane assembly, and camera electronics unit numbers, respectively.

Table 2. Camera-by-camera performance breakdown

Requirement	1Df (1)233)	Cf (C188)	Bf (1)306)	Af (A172)	An (A421)	Aa (A244)	Ba (11155)	Ca (C297)	Da (D3 i 09)
Boresight offset from nominal: ±8 pixel	-12.8	-8.7	(-1.6)	(1.6)	(1.4)	(5.'2)	(4.1)	(-5.())	(-1.3)
1 .ocaluniformity: less than ±3% deviation in response across each 4 pixel sc(. 1 .isted are the number of failed zones	27(1 at 1()%)	8 (5% max)	6 (1 at 14%; 1 at 10%)	7(1 at lx%; 1 at 12%)	15 (8% max)	33 (1 at 11%)	22(1 at 13%)	19(1 at 15%)	9 (1 at 24%)
Spectral, out-of-band (all fail 10^{-4}). Listed > $5x10^{-4}$	B3,4) $8x1()^{-4}$	B4) 6x10-4	B1) $6xi0^{-4}$	None	B4) $9x1()^{-4}$	None	N(mc	None	B2) $6xi()^{-4}$
Spectral, moments center wavelength: nominal±2 nm	B1: +5 B?: +3 114:-8	B1: +3 B2:+5 B4: -6	B1: +5 B2: +5 114:-3	B1: +5 B2: +5	B1: +3 B2: +3 114:-6	B1: +6 B2: +3 B4: -6	B1: +6 B2: +3 114:-5	B1: +4 B2: +5 B4: -3	B1: +4 B2: +4

In the first row, cross-track boresight is reported in parentheses where the specification was met. Two failures are noted, although they are small enough to have no performance impact. The second row reports the number of 4 pixel sets per camera (among the total of 1504 sets) in which local uniformity was violated. In parentheses are tallied the response deviation, in instances where a pixel set violated a 10% criteria, else the maximum deviation is noted. It is shown that the number of pixel sets that deviate by more than 10% is limited to 9 among 9 x 1504 sets. The third row lists those bands, B, R'here the out-of-band transmittance exceeded 5×10^{-4}, at one or more spectral wavelengths. It is known that the integrated out-in band ratio averaged 1, 2,5, 2, and 1.5% for the four spectral bands, respectively, reaching a maximum of 3.5% for two Band 2 channels. This out-of-band energy resulted in the center wavelength violations reported in row 4. Here the specification calls for computing center wavelength from a moments analysis of the total-band response. When a gaussian best-fi(to the in-band data is made, the computed center wavelength is within 3 am of nominal.

3. RADIOMETRIC CALIBRATION

This section will develop the functional form of the radiometric calibration equation used in MISR calibration anti Level 1 radiance processing, and present findings from radiometric calibration testing.

3.1 Photodiode standards

MISR is unique in that the radiometric scale is determined preflight and on-orbit using detector standards. As these standards are photoconductive devices, they produce a current in response to incident photons. For either the laboratory standards, used to calibrate the integrating sphere, or the flight standards, (his relationship can be expressed by:

$$i_\lambda = R_\lambda^{diode}\, q\, N_\lambda \tag{1}$$

1 Iere R_λ^{diode} is the product of the detector quantum efficiency, filler transmittance, and window transmittance, q the electron charge, and N_λ the photon rate. Next utilized is the energy per photos expression, $E_\lambda = hc/\lambda$, with h Planck's constant and c the speed of light. The photon rate is found as the ratio of incident flux, Φ_λ, to photon energy, where $\Phi_\lambda = L_\lambda A\Omega$ with L_λ the incident spectral radiance, and $A\Omega$ the detector etendue (area times flclci-of-view product). From these it is ciclct-mined that the spectral radiance of the calibration standard (sphere or flight diffuse panel) is

$$L_b^{diode} = 1.2395\ W\ \mu m\ Amps^{-1} \Big/ A\Omega \int_{200}^{1200} N_{\lambda,\,cal} R_\lambda^{diode} \lambda\, d\lambda \tag{2}$$

with $N_{\lambda,cal} = L_{\lambda,cal}/L_{b,cal}$ (**the** source spectral distribution, normalized by the value at the center wavelength). For preflight calibration we determine $N_{\lambda,cal}$ from the Planck blackbody function, at the bulb color temperature of 3100K; for flight calibration we utilize a model of the exo-atmospheric solar irradiance. The subscript b denotes a unique measure for each of the four MISR bands. The limits of integration encompass the photodiode response limits. It is noted that the measured quantity is a spectral radiance at the camera bandcenter (as determined by a moments analysis of the spectral response function).

3.2 CCD devices

The response of a CCD device, such as the MISR camera line arrays, can likewise be developed (in theory) from the relationship given in Eqn. 1, but includes the integration lime, 't', and analog-to-digital conversion factor, g (having units of digital number (DN) per electron). In practice, it has been determined that a quadratic calibration equation produces lower residuals for MISR, as compared to a linear approximation to the measured radiometric transfer curve. The equations in this section, therefore, do not represent the final transfer equation, but motivate the approach that will be more precisely defined in the next section. With this caveat, the camera DN is related to radiance by

$$DN = \frac{A\Omega T g}{hc} \int_{365}^{1100} L_\lambda R_\lambda \lambda d\lambda \tag{3}$$

where the cam era response, R_λ, includes the detector quantum efficiency, aad aay optical transmittance terms, including the filter and lens. The lower wavelength cat-ofl'01 365 nm is due to the lens/ optical element cut-off response. The upper limit, 1100 nm, is attributed to the detector cut-off, and is established from the band-gap of silicon,

It is noted that only the integral of the scene radiance, 1_λ, with the system response function, R_λ, can bc measured (in that the relative scene spectral profile is unknown). In order to retrieve a parameter that is independent of the instrument characteristics, an assumption as to the relative scene spectral profile would be needed. Rather, one could simply choose to retrieve a band-weighted radiance, denoted by the symbol $\mathcal{L}$. For MISR, however, there arc 9 x 15 (M different detector elements, hence response functions, for a given band. Wc choose to adopt a standardized spectral response function for calibration), $S_{\lambda,b}$, unique for each spectral band, b. This profile is created from the average of the measured profiles.

For calibration, then, wc regress radiance, $\mathcal{L}_{b,cal}^{std}$, against camera output DN where wc define

$$I_{b,cal}^{std} \equiv \left(\int_{365}^{1100} L_{\lambda,cal} S_{\lambda,b} \lambda d\lambda \right) \Big/ \left(\int_{365}^{1100} S_{\lambda,b} \lambda d\lambda \right) \tag{4}$$

This can be determined from the photodiode current via Eqns. 2 and 4:

$$I_{b,cal}^{std} = \frac{i}{A\Omega} \frac{1.2395}{\int_{365}^{1100} S_{\lambda,b} \lambda d\lambda} \left(\int_{365}^{1100} N_{\lambda,cal} S_{\lambda,b} \lambda d\lambda \right) \Big/ \left(\int_{365}^{1100} N_{\lambda,cal} R_\lambda^{diode} \lambda d\lambda \right) \tag{5}$$

The last Iwo terms in parentheses adjust for the spectral differences between the photodiode standard and the assumed camera response profile. II is noted that even with photodiode and camera filters of the same design, the response functions arc quite different due to differences in quantum efficiency and spectral transmittance of the respective optical elements.

With this input the cameras arc. calibrated via a regression of the foi m

$$DN = G^{std} \mathcal{L}_{b,cal}^{std}. \tag{6}$$

From the model presented in Eqn. 3, and Eqn. 4, it can be shown that

$$G^{std} = \frac{A\Omega T g}{hc} \left(\int_{365}^{1100} S_\lambda \lambda d\lambda \right) \left(\int_{365}^{1100} N_{\lambda,cal} R_\lambda \lambda d\lambda \right) \Big/ \left(\int_{365}^{1100} N_{\lambda,cal} S_\lambda \lambda d\lambda \right) \tag{7}$$

This coefficient G^{std} is used for scene radiance retrieval. As no correction is made for specific pixel response differences, the retrieved radiances will only approximate the desired measure of a radiance weighted by the standardized response profile. The retrieved radiance, $\mathcal{L}^{ret}$, can bc found to be

$$L^{ret} = \frac{DN}{G^{std}} = \left[\left(\int_{365}^{1100} L_{\lambda,scene} R_\lambda \lambda d\lambda \right) \Big/ \left(\int_{365}^{1100} S_\lambda \lambda d\lambda \right) \right] \left(\int_{365}^{1100} N_{\lambda,cal} S_\lambda \lambda d\lambda \right) \Big/ \left(\int_{365}^{1100} N_{\lambda,cal} R_\lambda \lambda d\lambda \right) \tag{8}$$

When the normalized scene spectral shape equals that of the calibration source ($N_{\lambda,scene} = N_{\lambda,cal}$) we have

$$L_b^{ret} = \left(\int_{365}^{1100} L_{\lambda,scene} S_\lambda \lambda d\lambda \right) / \left(\int_{365}^{1100} S_\lambda \lambda d\lambda \right) \quad L_{b,scene}^{std} \tag{9}$$

That is, to the extent the scene spectral shape matches that of the calibration source, the retrieved radiance is the desired parameter, $L_{b,scene}^{std}$. This is a good approximation for spectrally flat scenes. The retrieved radiance is likewise found to approximate the desired measure, for arbitrary scene profiles, when the measured and standardized spectral response functions are nearly identical. It has been shown that the difference between the actual retrieved radiance (modeled by Eqn. 8) and the desired measure (Eqn. 9) is less than a percent at low scene reflectances, and is negligibly small at more typical radiance levels[7].

It is noted that a different approximation profile $S_{\lambda,b}$ could have been selected. If, for example, $S_{\lambda,b}$ had been defined as the in-band portion of the measured spectral response profile, errors on the order of several percent in retrieved radiance would be made[7]. For this reason MISR characterizes the out-of-band response of the detectors, and makes a correction to provide the in-band weighted radiance. This is done for certain Level 2 products where accuracy warrants the processing.

3.3 Calibration equation

As stated above, it has been empirically determined that a quadratic functional form of the radiometric calibration equation produces lower residuals to the calibration observations. The relationship used, therefore, in calibration and Level 1 radiance retrieval is:

$$G_2 (L_b^{std})^2 + G_1 L_b^{std} + G_0 = DN - DN_0 \tag{10}$$

where
- L_b^{std} is the incident radiance, weighted by a standardized band response profile [W m^{-2} sr^{-2} μm^{-1}],
- DN is the camera digital number,
- G_2, G_1, and DN_0 are best fit parameters to the measured radiative transfer curve, and
- DN_0 is the video offset voltage, unique for each line of data, and measured by the overclock pixels for that line.

Preflight calibration has determined that, for the MISR cameras, the CCD response is nearly linear, and the coefficients G_0 and G_2 are quite small. Inclusion of these terms improves the radiance retrieval at the lowest end of the detector transfer curve.

Figures 1 and 2 plot the response of each pixel and camera, as determined from preflight radiometric calibration. (Plotted is the coefficient G_1, when a linear fit to the calibration data is made). Local deviations in response, discussed in the above section, are shown to be small. Differences in field angle and spectral band are noted. One manufacture error, for Camera Ba, is noted. Here, the filter was mistakenly cut perpendicular to lines of equal deposition radius, and a greater transmittance variation across the array is noted.

Figure 3 provides the saturation limit (i.e., the minimum scene equivalent reflectance which saturates a given detector element), for various positions across each channel. Differences are a direct result of the response variation across the array. In selecting an integration time for a given channel, signal-to-noise ratio (SNR) and saturation limit are considered. specifically, the integration time is determined such that the SNR specifications are just met at the edge-of-field. For all but some Band 4 channels at the edge-of-field, there is a large margin between an equivalent reflectance of unity, $\rho_{eq}=1$, and the saturation limit.

4. SPECTRAL CALIBRATION

As was mentioned in the section above, the measured spectral response profiles are used to derive band-standardized profiles. These latter response functions, and the measured laboratory and flight photodiode profiles, are used in the radiometric

calibration algorithm (Eqns. *5).* Additionally, analyses of the spectral response functions can lead to descriptor parameters to the actual functions. These derived parameters are a mathematical convenience, and useful in (Mining specifications, in comparing }Jixcl-lo-pixel or camera-to-camera response differences, or in assigning a wavelength to which a geophysical parameter (e.g., surface reflectance, or atmospheric transmittance) is reported. The gaussian representation is useful in approximating the MISR in-band region. This is because the MISR filters were designed to be gaussian in shape, allowing a polarization insensitive camera design when used in conjunction with a Lyot depolarizer. A computation of peak response, $R_{g,p}^{\text{in-band}}$. CcIllCl' wavelength, $\lambda_{g,p}^{\text{meas,in-band}}$ and full-width-half-maximum (FWHM), $\Delta\lambda_{g,p}^{\text{meas,in-band}}$, is made to provide a response representation of the form

$$R_{\lambda g,p}^{\text{in-band}} = R_{g,p}^{\text{in-band}} \exp[-(4 \ln 2)\ (\lambda-\lambda_{g,p})^2/\Delta\lambda_{g,p}^2] \qquad (11)$$

Results of Ibis parameterization are shown in Figure 4. The average center wavelength for each band fall no more than 2 nm from the specified values. Note that out-of-band response dots not contribute to these in-band parameters.

5. SUMMARY

Preflight testing bas determined that the MISR cameras have met their design specification for the majority of parameters. Calibration data have been acquired and used to derive gain coefficients, assuming a quadratic approximation to the measured radiometric transfer curve. Knowledge of the calibration detector standard's spectral response, as well as a band-standardized camera spectral response, is used in this radiometric calibration process. With the derived gain coefficients, Level 1 data processing provides scene radiances, averaged over a band-standardized spectral response function. I .evel 1 processing will also utilize image restoration, using a PSF deconvolution routine, to reduce the radiometric error for spatially inhomogeneous scenes. In 1 .evel *2* processing, spectral data arc used to provide an out-of-band correction for certain products. This reduces radiometric error (in that only an in-band response is desired) from a fcw percent, 10 less than a percent.

6. ACKNOWLEDGMENTS

The design, fabrication, anti characterization of the MISR instrument is credited to a large number of individuals. The calibration and characterization tests described in this text have been developed with the assistance of S. Teré Smith (camera and system test engineer), Valerie G.Duval, Daniel J. Preston, and Ghobad Saghri (calibration engineering), Eric B. Hochberg, Daniel M. Kirby, and Cesar Sepulveda (optical testing), Neil D. Pignatano (Ground Support Equipment), Mary J.. White (lens fabrication and test), Enrique B. Villegas (CCD fabrication anti test), and David J. Diner (principal investigator). The work described in this paper is being carried out by the Jet Propulsion Laboratory, California Institute of Technology, under contract with the National Aeronautics and Space Administration.

7. REFERENCES

1. Bruegge, C. J., D.J. Diner, and V.G. Duval (1996). The MISR calibration program. J. of Atmos. and oceanic Tech., Vol. 13(2), 286-299.

2. Bruegge, C.J., V.G. Duval, N. L. Chrien, anti R. f'. Korechoff (1995). MISR instrument development and lest status. in *Advanced and Next-Generation Satellites.* Proc. EUROPTO/SPIE, Vol. **2538**, 92-103, Paris, France, 25-28 September.

3. Bruegge, C. J., V.[i. Duval, N.L. Chrien, and D.J. Diner (1993). Calibration Plans for the Mui(i-angle imaging SpectroRadiometer (MISR). Metrologia, 30(4), 213-221.

4. Korechoff, R., 1). Kirby, E. Hochberg, C. Sepulveda, and V. Jovanovic (1996). Distortion calibration of the MISR linear detectors. in *Earth Observing System,* Proc. S1'1 i E, Vol. 2820, 1 Denver, Colorado, 5-9 August.

5. Hochberg, E.B., M.L. White, R.P. Korechoff, and C.A. Sepulveda (1996). Optical testing of MISR lenses and cameras. In *Optical Spectroscopic Techniques and Instrumentation for Atmospheric Space Research* II. *Proc.* SPIE, Vol. **2830**, Denver, Colorado, 5-9 August.

6. Bruegge, C. J., R.M. Woodhouse, D.J. Diner (1996). In-flight radiometric calibration plans for the Earth Observing System Mul[i-angle Imaging SpectroRadiometer, IEEE/IGARSS, Paper No. 96.1028, Lincoln, Nebraska, 27-31 May.

7. Chrien, N.L., C.J. Bruegge (1996). Out-of-band spectral correction algorithm for the Multi-angle Imaging SpectroRadiometer. In *Earth Observing System*, Proc. SPIE, Vol. **2820**, Denver, Co, 5-9 August.

8. Korechoff, R.P, D.J. Diner, D.J. Preston, C.J. Bruegge (1995). Spectroradiometer focal-plane design considerations: lessons learned from MISR camera testing. In *Advanced and Next-Generation Satellites*. Proc. *1[UI{O1''1'[VS1'111,* Vol. **2538**, 104-11 6, Paris, France, 25-28 September.

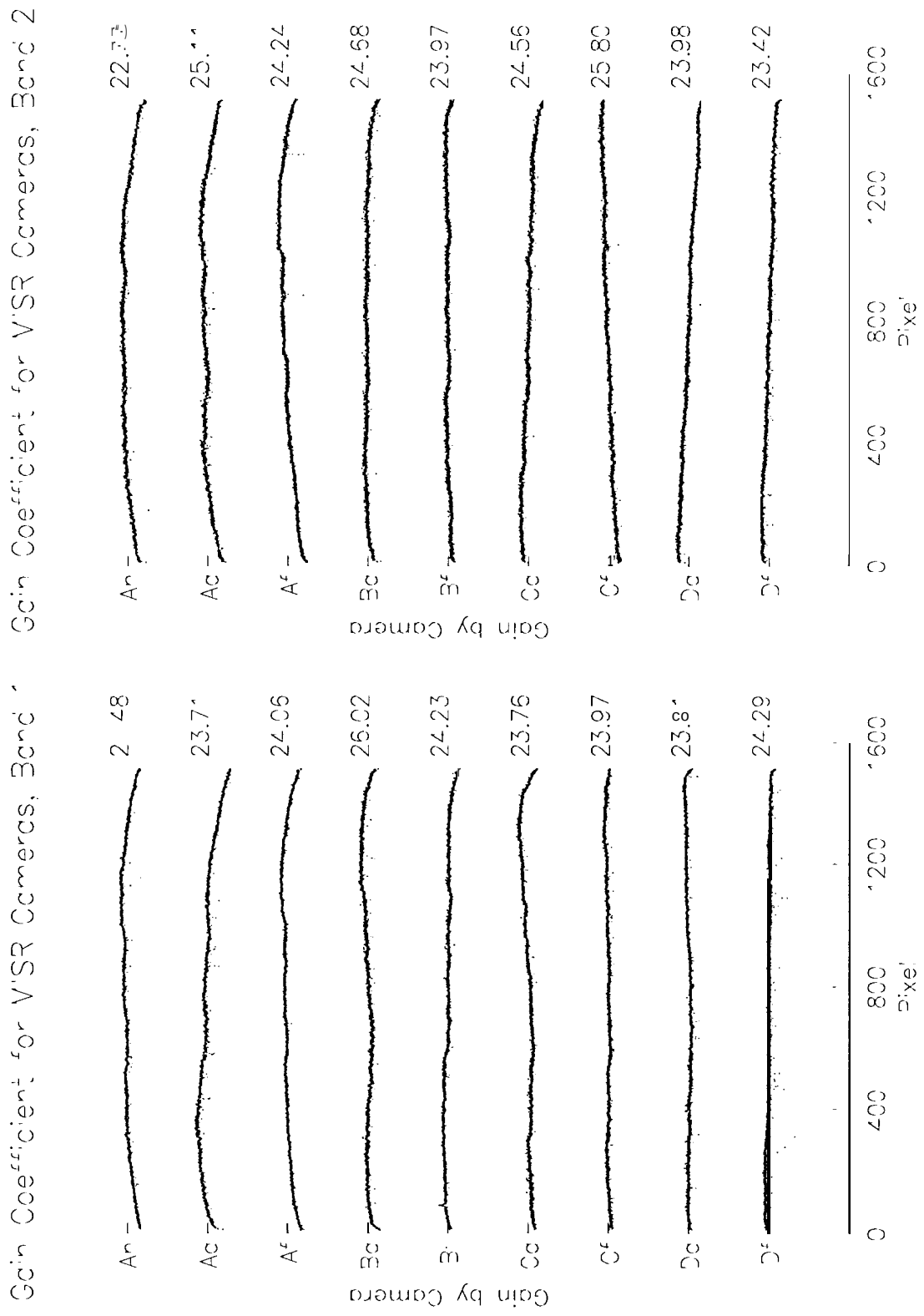

Figure 1. Bands 1 and 2: Detector response per channel and field-angle.

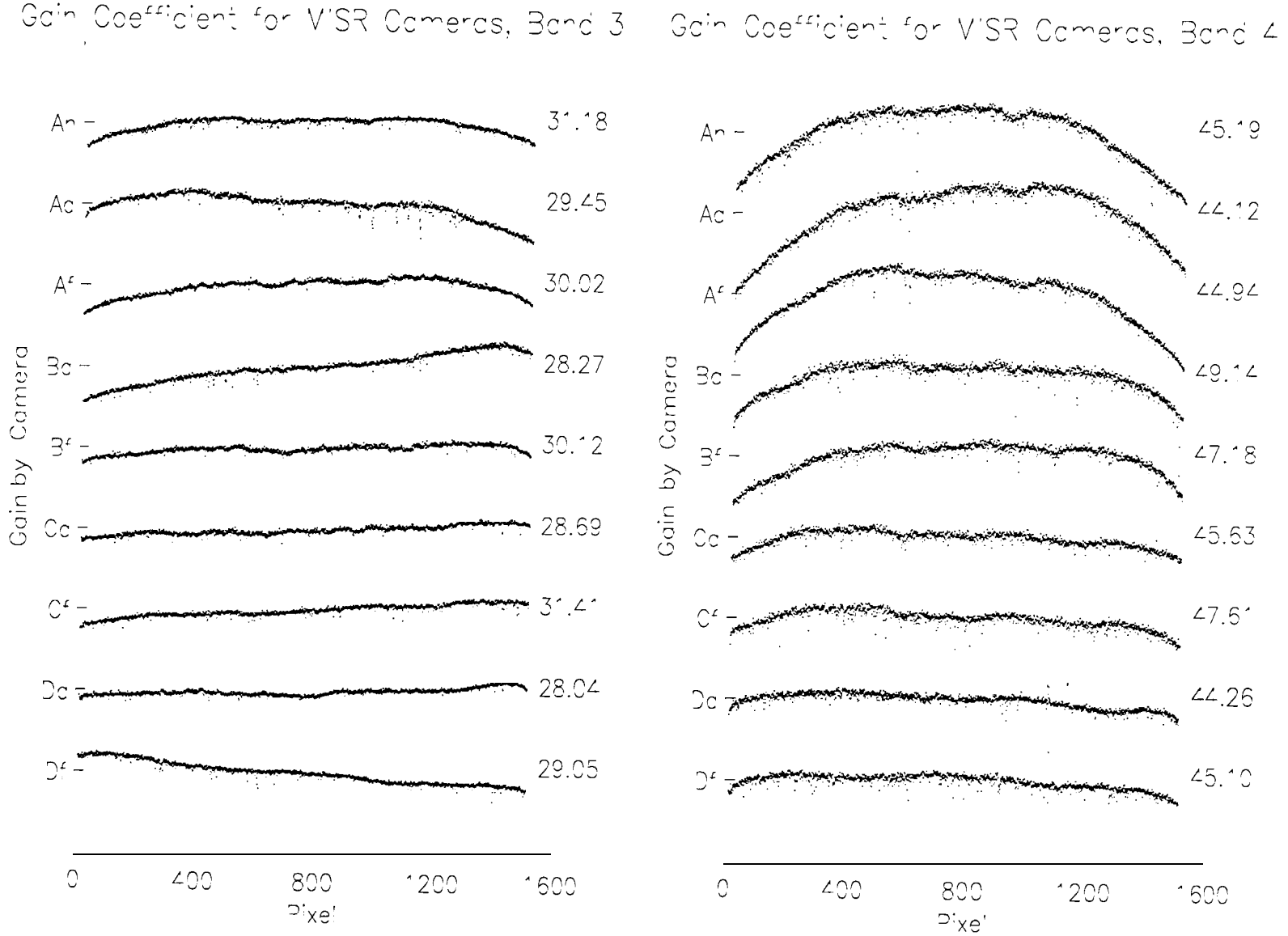

Figure 2. Bands 3 and 4: Detector response per channel and field-angle.

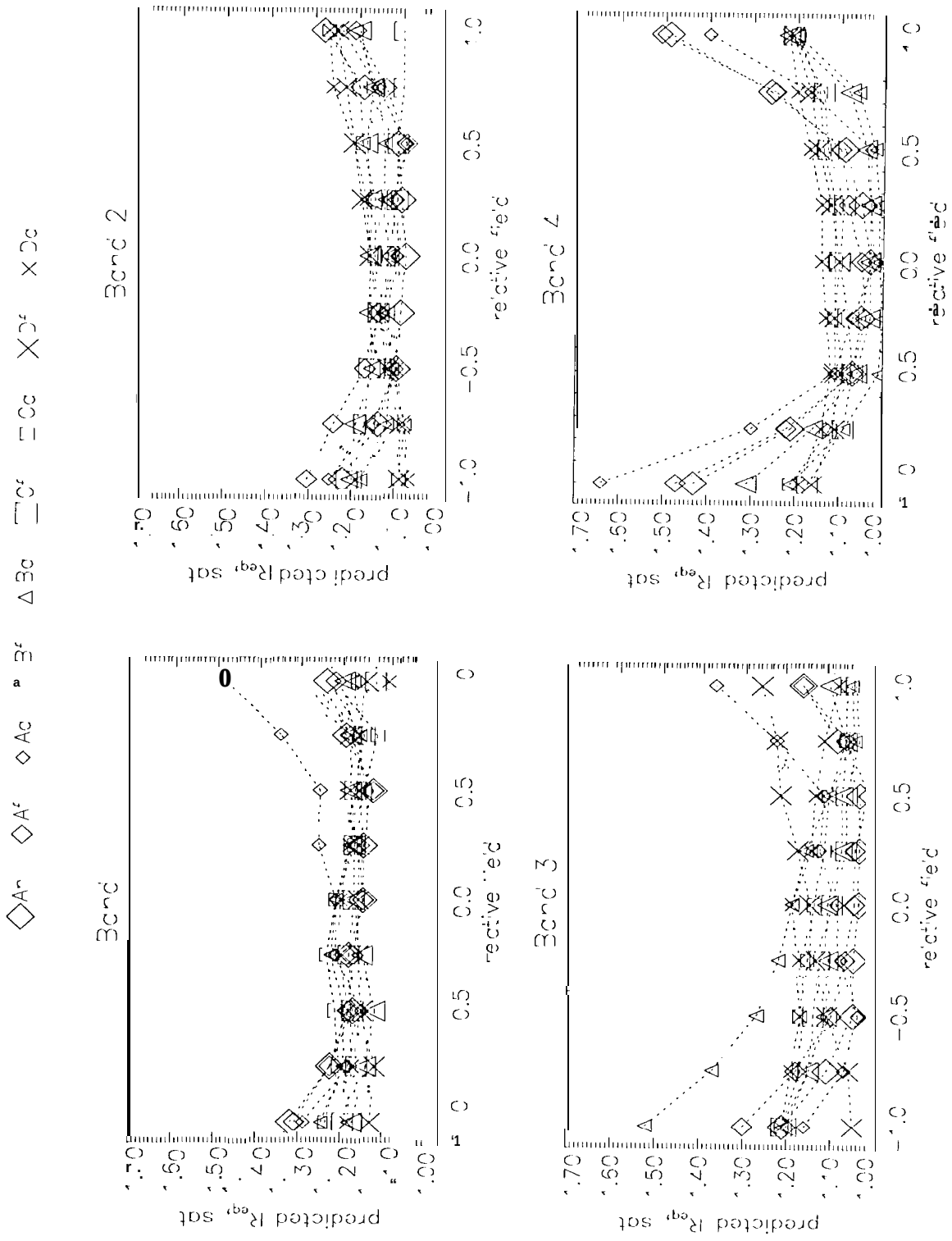

Figure 3. Saturation values per channeland fic](1-angle.

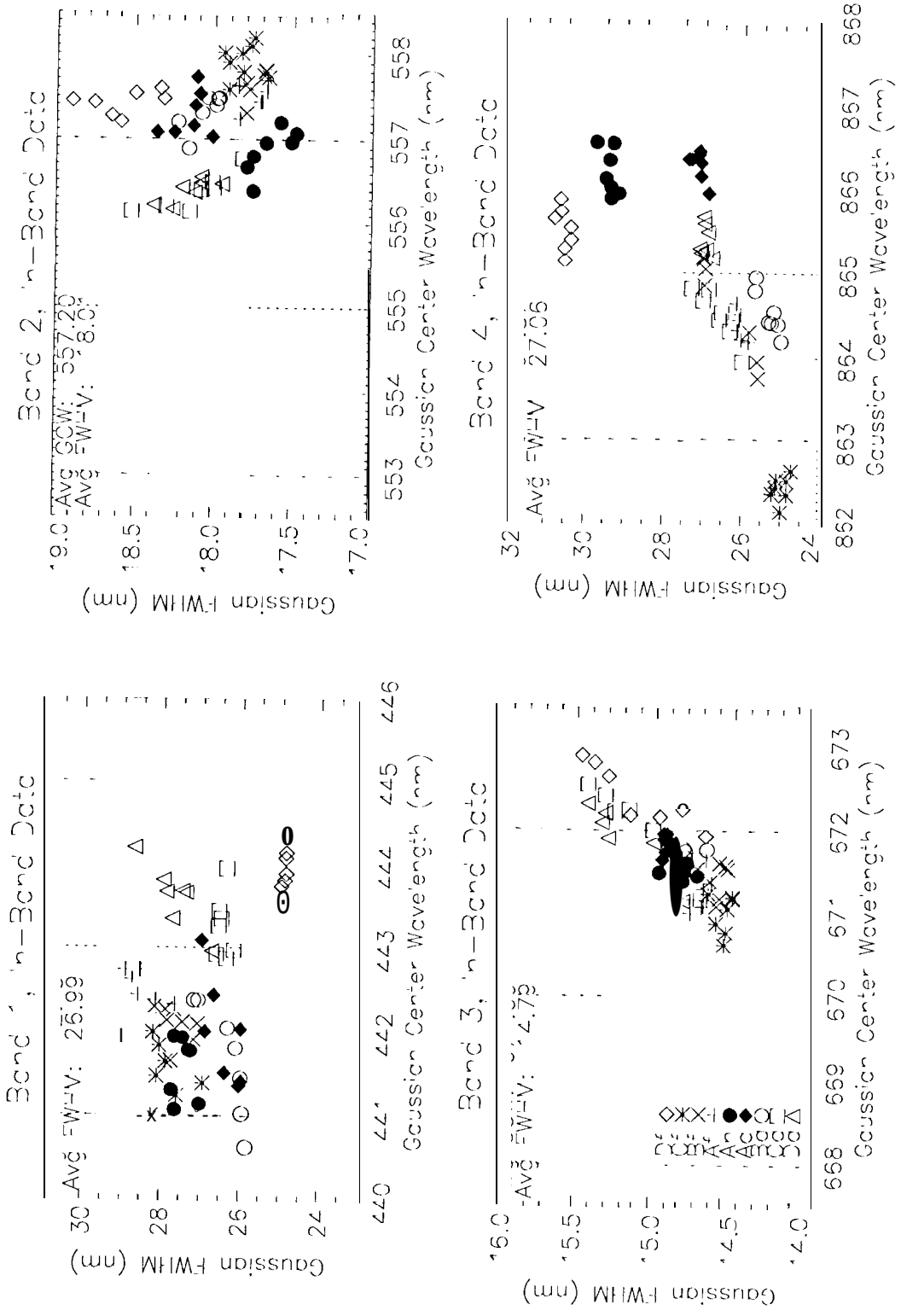

Figure 4. Best-fil gaussian analysis to the in-band spectral response profiles, at discrete field positions (legend provided within Band 3 plot).